

VELOCITY DISPERSIONS OF CNOC CLUSTERS  
AND THE EVOLUTION OF THE CLUSTER ABUNDANCE

STEFANO BORGANI<sup>1 2</sup>, MARISA GIRARDI<sup>3</sup>, RAY G. CARLBERG<sup>4 5</sup>  
HOWARD K.C. YEE<sup>4 5</sup> AND ERICA ELLINGSON<sup>5 6</sup>

ABSTRACT

We present the results of the analysis of the internal velocity dispersions,  $\sigma_v$ , for the sample of 16 distant galaxy clusters ( $0.17 \lesssim z \lesssim 0.55$ ) provided by the Canadian Network for Observational Cosmology (CNOC). Different  $\sigma_v$  estimates are provided, all based on an interlopers removal algorithm, which is different from that originally applied by Carlberg et al. (1996). We find that all such methods provide  $\sigma_v$  estimates which are consistent within  $< 10\%$  among themselves and with the original estimates provided by the CNOC collaboration. This result points in favor of a substantial robustness of currently applied methods for optical studies of the internal cluster dynamics. The resulting distribution of velocity dispersions is used to trace the redshift evolution of the cluster abundance with the aim of constraining the matter density parameter,  $\Omega_m$ . We find that constraints on  $\Omega_m$  are very sensitive to the adopted value of  $\tilde{\sigma}_8 = \sigma_8 \Omega_m^\alpha$  ( $\alpha \simeq 0.4-0.5$ ), as constrained by the local cluster abundance. We find that, as  $\tilde{\sigma}_8$  varies from 0.5 to 0.6, the best fitting density parameter varies in the range  $0.3 \lesssim \Omega_m \lesssim 1.0$ . A further source of uncertainty in constraining  $\Omega_m$  is due to uncertainties in the correction for the  $\sigma_v$ -incompleteness of the CNOC sample. This calls for the need of better understanding the constraints from the local cluster abundance and increasing the statistics of distant clusters in order to suppress the systematics related to the sample completeness criteria.

*Subject headings:* Cosmology: galaxies - clusters - theory - large-scale structure of the universe.

1 INTRODUCTION

Galaxy clusters represent the virialization stage of exceptionally high peaks of initial density perturbations on comoving scales of about  $10 h^{-1} \text{Mpc}^7$ . Therefore, their abundance is sensitive to the amplitude of the fluctuation power spectrum on such scales. Standard analytical methods based on the approach originally devised by Press & Schechter (1974, PS hereafter) show that the number density of clusters of a given mass provides a robust constraint on  $\tilde{\sigma}_8 = \sigma_8 \Omega_m^\alpha$ , where  $\sigma_8$  is the r.m.s. fluctuation amplitude within a sphere of  $8 h^{-1} \text{Mpc}$  radius,  $\Omega_m$  is the matter density parameter and  $\alpha \simeq 0.4-0.5$ , weakly dependent on  $\Omega_m$ , on the presence of a cosmological constant term and on the shape of the power-spectrum (e.g., White, Efstathiou & Frenk 1993).

However, while theoretical predictions provide the number density of clusters as a function of their mass, observations give the cluster abundance as a function of some observable quantity, like the  $X$ -ray luminosity, the  $X$ -ray temperature or the velocity dispersion of member galaxies, which are *a posteriori* connected to mass at different degrees of reliability. Despite the variety of methods and of data sets employed to trace the local cluster abundance, all the analyses consistently indicate that  $\tilde{\sigma}_8 \simeq 0.5-0.6$  (Eke et al. 1996; Kitayama & Suto 1997; Oukbir, Bartlett

& Blanchard 1997; Girardi et al. 1998a; Pen 1998; Markevitch 1998; Borgani et al. 1999, B99 hereafter; Viana & Liddle 1999). Once a model is tuned so as to reproduce the abundance of local clusters, its evolution mainly depends on  $\Omega_m$  (e.g., Oukbir & Blanchard 1992). Therefore, having a statistical sample of high-redshift clusters with reliable mass determinations would allow in principle to break the degeneracy between  $\Omega_m$  and  $\sigma_8$ .

The growing availability of high-redshift cluster samples selected in the  $X$ -ray band led in the last few years to a flurry of activity along this line. Using the redshift distribution of clusters from the Einstein Medium Sensitivity Survey (EMSS, Gioia et al. 1990), Sadat, Blanchard & Oukbir (1998) found consistency with a critical-density ( $\Omega_m = 1$ ) Universe (cf. also Reichart et al. 1999). B99 analyzed the ROSAT Deep Cluster Survey (RDCS, Rosati et al. 1995, 1998) and pointed out that current uncertainties in the evolution of the mass-luminosity relation prevent one from obtaining strong conclusions on  $\Omega_m$  even from a flux-limited sample as deep as RDCS ( $z \lesssim 1$ ).

In this respect, the possibility of measuring  $X$ -ray cluster temperatures would circumvent this problem to a fair degree, since it is more directly connected to the mass than the  $X$ -ray luminosity. Indeed, Eke et al. (1998) analyzed the Henry (1997) sample of  $X$ -ray cluster temperatures,

<sup>1</sup> INFN, Sezione di Perugia, c/o Dipartimento di Fisica dell'Università, via A. Pascoli, I-06123 Perugia, Italy

<sup>2</sup> INFN, Sezione di Trieste, c/o Dipartimento di Astronomia, Università degli Studi di Trieste, via Tiepolo 11, I-34131 Trieste, Italy; borgani@ts.astro.it.

<sup>3</sup> Dipartimento di Astronomia, Università degli Studi di Trieste, via Tiepolo 11, I-34131 Trieste, Italy; girardi@ts.astro.it.

<sup>4</sup> Department of Astronomy, University of Toronto, Toronto ON M5S 3H8, Canada; carlberg@astro.utoronto.ca., hyee@astro.utoronto.ca.

<sup>5</sup> Visiting Astronomer, Canada-France-Hawaii Telescope, which is operated by the National Research Council of Canada, Le Centre National de Recherche Scientifique, and the University of Hawaii

<sup>6</sup> Center for Astrophysics and Space Astronomy, University of Colorado, Boulder, CO 80309, U.S.A.; e.elling@casa.colorado.edu.

<sup>7</sup> Here  $h$  is the Hubble constant in units of  $100 \text{ km s}^{-1} \text{ Mpc}^{-1}$ .

extending out to  $z = 0.33$ . They concluded that the  $X$ -ray temperature function (XTF) favor a low-density Universe, with  $\Omega_m \simeq 0.4 \pm 0.2$ . Quite remarkably, Viana & Liddle (1999) analyzed the same data set and claimed that, after accounting for systematics in both the data set and in the theoretical PS framework, a critical density Universe is still viable as far as the evolution of the XTF is concerned.

It is clear that such ambiguities can in principle be eliminated by resorting to cluster data at a substantially higher redshift, where differences among different Friedmann geometries rapidly increase. However, the price to be paid in this case is that a much smaller number of clusters with highly accurate data is presently available (e.g., Luppino & Gioia 1995; Donahue et al. 1998; Rosati et al. 1999).

An alternative way to trace the cluster mass function back in redshift is offered by measurements of the velocity dispersions,  $\sigma_v$ , of member galaxies. This represents a well established technique, which has been already extensively applied to samples of local clusters (e.g., Zabludoff, Huchra, & Geller 1990; Girardi et al. 1993; den Hartog & Katgert 1996; Fadda et al. 1996; Mazure et al. 1996; Borgani et al. 1997, and references therein).

Systematic estimates of the velocity dispersions for a statistical sample of distant clusters has been performed for the first time by Carlberg et al. (1996, C96 hereafter). They analyzed the Canadian Network for Observational Cosmology (CNOC) sample of clusters (Yee, Ellingson & Carlberg 1996), which includes 15  $X$ -ray selected clusters from EMSS and Abell 2390. Carlberg et al. (1997b, C97 hereafter) used the CNOC sample to trace the evolution of the cluster abundance and concluded that  $\Omega_m$  values below unity are in general to be preferred (see also Bahcall, Fan & Cen 1997). However, this result depends sensitively on (a) the  $z \simeq 0$  normalization from the number density of local clusters with velocity dispersion above a given value, and (b) on the procedure to convert the distribution of cluster velocity dispersions into the distribution of cluster masses. In particular, one of the questions raised by C97 concerned the comparison between the different algorithms applied to estimate  $\sigma_v$  for local clusters and for the distant CNOC clusters. If the estimator used for local clusters provides  $\sigma_v$  which are biased upwards, this would give an overestimate of  $\bar{\sigma}_8$  and, therefore, of  $\Omega_m$ .

A reliable estimate of  $\sigma_v$  faces several problems, such as the presence of foreground and background interlopers, velocity anisotropy in galaxy orbits, the presence of substructures and the limited amount of data available. Girardi et al. (1993) showed that different methods presented in the literature to estimate  $\sigma_v$  (Yahil & Vidal 1977; Zabludoff, Huchra & Geller 1990; Beers, Flynn & Gebhardt 1990) give similar results on well sampled clusters, while only the robust estimator by Beers et al. (1990) seems to be efficient when only  $\sim 10$  galaxy redshifts per cluster are available. Besides the estimate of  $\sigma_v$  from redshifts of member galaxies, a further critical issue concerns the identification of genuine cluster members by removing foreground and background interlopers.

For instance, Girardi et al. (1993) rejected interlopers

by following a guess for the outer limits of the redshift range encompassed by each cluster. Two different, more refined, methods for interloper removal have been subsequently developed by Fadda et al. (1996, F96 hereafter; see also Girardi et al. 1998b, G98 hereafter) and by den Hartog & Katgert (1996; see also Adami et al. 1996; Mazure et al. 1996), both based on combining information on projected position and velocity of each galaxy, although by using rather different procedures. Quite remarkably, such procedures of cluster member selection lead to velocity dispersions which are in good agreement (cf. F96 and Adami et al. 1998). Significant differences were found only for a small number of clusters (8 out of 74) which were recognized by the procedure of F96 as multiple structures in redshift space.

Despite their differences, a common feature of all such methods is that they are based on the identification of individual interlopers to be removed. Quite differently, the method followed by C96 to estimate  $\sigma_v$  for CNOC clusters statistically subtract the mean density of field galaxies from the redshift space of the cluster. The resulting velocity dispersions, which are about 13% lower than without the background subtraction, have been shown by Mushotzky & Scharf (1997) to be in good agreement with those inferred from the  $X$ -ray temperatures provided. Furthermore, Lewis et al. (1999) have shown that virial masses for CNOC clusters are quite consistent with those obtained from  $X$ -ray data analysis.

In this paper, we perform a complete re-analysis of the cluster velocity dispersion of the CNOC sample by applying different algorithms which are similar to that used by F96 for local clusters. Such estimates of the velocity dispersions will be used to estimate the evolution of the cluster abundance through the redshift-dependence of the  $\sigma_v$  distribution.

Therefore, the final goal of this paper will be to answer to the following two questions. (a) Does the explicit background subtraction method, applied by C96 to estimate  $\sigma_v$  for CNOC clusters, provide consistent results to those from methods applied by F96 and G98 to local cluster samples? (b) Having a reliable determination of velocity dispersions for a sample with the statistics and the redshift extension of CNOC, are we able to provide robust constraints on  $\Omega_m$  from the evolution of the cluster abundance?

The structure of the paper is as follows. In Section 2 we briefly describe the CNOC sample. In Section 3 we introduce the different methods to estimate  $\sigma_v$ . After showing the results of the application to the CNOC clusters, we compare the results to those provided by C96 (cf. also Carlberg et al. 1997a). In Section 4 we use such results on  $\sigma_v$  to place constraints on  $\sigma_8$  and  $\Omega_m$ . We draw our main conclusions in Section 5.

## 2 THE CNOC SAMPLE

A comprehensive description of the CNOC cluster sample is provided by Yee, Ellingson & Carlberg (1996). In the following we only describe the main features which are rele-

vant to our analysis, while we refer to that paper for a more complete presentation. The CNOC cluster redshift survey includes all the 15 EMSS clusters (Gioia et al. 1990; Henry et al. 1992) which have  $L_X > 4 \times 10^{44} \text{ erg s}^{-1}$  ( $h = 0.5$  and  $q_0 = 0.5$ ) and  $f > f_{lim} = 4 \times 10^{-13} \text{ erg s}^{-1} \text{ cm}^{-2}$  for  $X$ -ray luminosities and fluxes in the  $[0.3, 3.5]$  keV energy band, redshift in the range  $[0.17, 0.55]$  and  $-15^\circ < \delta < +55^\circ$  for the declination. The solid angle covered by EMSS in this declination range is of 587 sq. deg. Also included in the original CNOC sample is Abell 2390, which however does not belong to EMSS. Although it is included in our  $\sigma_v$  analysis, we will not use it for the purpose of constraining cosmological models.

The CNOC surveys provided a fairly large number (50 to 200) of galaxy redshifts per cluster over a region covering up to  $6 h^{-1} \text{ Mpc}$  projected on the sky. Galaxy magnitude selection criteria have been chosen so as to minimize contamination due to foreground/background objects. This makes the CNOC clusters very well suited to follow the redshift evolution of the cluster internal dynamics.

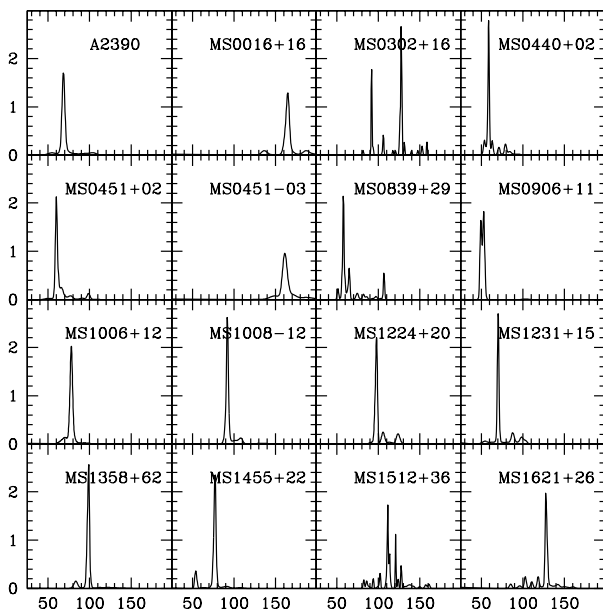


Fig. 1.— The velocity–space galaxy density, as provided by the adaptive–kernel reconstruction method. Units on the  $x$ -axis are velocities in  $10^3 \text{ km s}^{-1}$ , while the  $y$  axis is in arbitrary units.

### 3 ANALYSIS OF THE CNOC SAMPLE

In order to select member galaxies and compute velocity dispersions,  $\sigma_v$ , we apply the same procedure adopted by F96 and G98 for nearby clusters. We remind that the other recent  $\sigma_v$  analysis for an extended sample of nearby clusters (Mazure et al. 1996) leads to velocity dispersions

which are in good agreement, although it resorted to a different procedure for the selection of cluster members (cf. F96 and Adami et al. 1998).

#### 3.1 Cluster Member Selection

The member selection for the CNOC clusters is performed by considering the whole sampled region around each cluster, with the exception of MS1512+36, which we analyze only within  $1 h^{-1} \text{ Mpc}$ . This cluster appears as very elongated and shows strong complexity in the two dimensional galaxy distribution. Therefore, we prefer to avoid distant cluster regions where this complexity makes difficult a dynamical analysis (see below). The initial list of candidate cluster members do not include galaxies which are very far from the cluster redshift range and, therefore, are clearly foreground/background objects.

The identification of cluster members proceeds in two steps.

Firstly, we perform the cluster membership selection in velocity space by using only redshift information. We use the adaptive kernel method (Pisani 1993) to find the significant ( $> 99\%$  c.l.) peaks in the the velocity distribution. Only galaxies belonging to such peaks are considered as candidate cluster members. In Figure 1 we plot the velocity–space galaxy density for all the CNOC clusters, as provided by the adaptive–kernel reconstruction method.

From the above member selection analysis only the MS0906+11 cluster, shows two significant peaks, which are separated by  $> 3000 \text{ km s}^{-1}$  in velocity space (hereafter MS0906+11a and MS0906+11b). According to our procedure, these two peaks show a significant overlapping ( $> 40\%$ ) and they are not perfectly separable, thus leading to a cluster with uncertain dynamics. The amount of evidence of this binary nature (e.g. C96; Carlberg et al. 1997a), as well as the strong disagreement between  $\sigma_v$  of the whole system ( $1723 \text{ km s}^{-1}$  from the present analysis and  $1893 \text{ km s}^{-1}$  from C96) and the  $X$ -ray temperature reported by Lewis et al. (1999;  $8 \text{ keV}$ , corresponding to  $\sim 1150 \text{ km s}^{-1}$  under the hypothesis of energy equipartition between gas and galaxies), indicates that this cluster should be better considered as composed of two separated peaks.

Also the velocity distribution of MS1512+36 is very complex. The cluster peak is surrounded by secondary peaks, which have a smaller density and are separated from the main peak. This complexity further motivates our choice to estimate  $\sigma_v$  for this cluster only within  $1 h^{-1} \text{ Mpc}$ .

All those galaxies which pass through the first velocity–space selection are analyzed in the second step, which uses the combination of position and velocity information. This procedure, which is based on the “shifting gapper” algorithm, proceeds in two iterative steps. Firstly, galaxies are assigned to radial bins of  $0.4 h^{-1} \text{ Mpc}$  width or larger, in order to contain at least 15 objects. Secondly, those galaxies that, within each bin, are separated in cluster rest–frame velocity by  $\geq 1000 \text{ km s}^{-1}$  from the main body of the velocity distribution are identified as interlopers. These two steps are iterated until the number of cluster members

does not change anymore. Figure 2 shows the plots of rest-frame velocity versus projected cluster-centric distance for those clusters where the “shifting gapper” found interlopers (indicated with the open circles). We note that the MS1358+62 cluster contains a close system, which corresponds to a southern group identified in velocity space and already noted by C96 (the vertical line mark the separation between these two systems). In order to exclude this secondary structure, hereafter we analyze the MS1358+62 cluster only within  $1.2 h^{-1}\text{Mpc}$ .

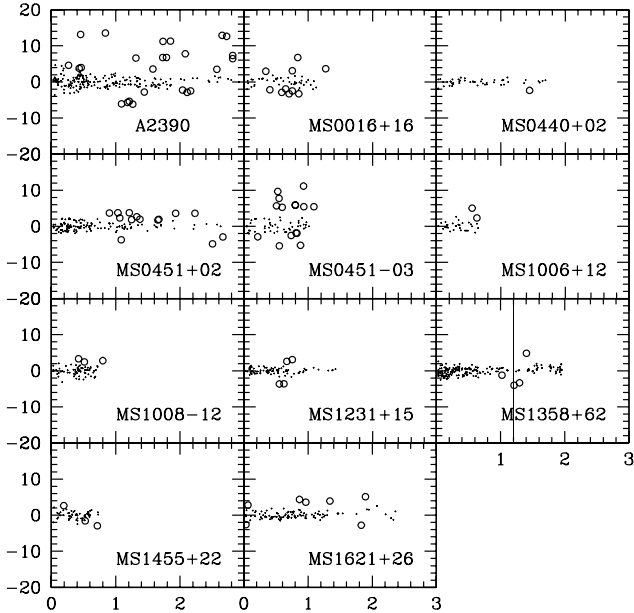


Fig. 2.— Rest-frame velocity versus projected cluster-centric distance for each cluster where the “shifting gapper” succeeded in rejecting at least one galaxy. Distances on the  $x$ -axis are in units of  $h^{-1}\text{Mpc}$  and the rest-frame velocities on the  $y$ -axis are in units of  $10^3 \text{ km s}^{-1}$ . Interlopers are indicated with the open circles. As for the MS1358+62 cluster, the thin vertical line marks the separation between the main cluster and a nearby subgroup (see text).

Finally, we estimate the corrections for velocity gradients, which are however always quite small (e.g. Girardi et al. 1996). We verify that only A2390 has significant (at  $> 99\%$  c.l.) velocity gradients. For this cluster we apply a correction by subtracting the velocity gradient from each galaxy velocity and renormalizing the velocities so as to have their mean velocity unchanged. This correction results in a decrease of  $\sigma_v$  (see below) by  $58 \text{ km s}^{-1}$ .

### 3.2 The velocity dispersion estimation

We compute robust estimates of (line-of-sight) velocity dispersions,  $\sigma_{rob}$ , by using the ROSTAT routines by Beers, Flynn, & Gebhardt (1990), after applying the relativistic correction and the usual correction for velocity

errors (Danese, De Zotti, & di Tullio 1980). We use the bi-weight scale estimator when more than fifteen member galaxies are available, while the gapper estimator is applied otherwise (see also Girardi et al. 1993),

Several authors (F96; den Hartog & Katgert 1996; Girardi et al. 1996) have shown that velocity dispersion profiles for individual clusters are often a strong, either increasing or decreasing, function of the radius in the central cluster regions. This behavior may be due both to velocity anisotropies and to the dark matter distribution, although it is not easy to disentangle between these two effects (e.g., Merritt 1987). However, most integrated profiles,  $\sigma_v(< R)$  (i.e.,  $\sigma_v$  evaluated by using the all the galaxies within the projected radius  $R$ ), become flat in the external cluster regions (F96; Girardi et al. 1996). This suggests that possible velocity anisotropies does not significantly affect the value of  $\sigma_v$  when it is estimated over a wide cluster region, so as to be representative of the total kinetic energy.

Figure 3 shows the integrated velocity dispersion profiles,  $\sigma_v(< R)$ , for all the CNOC clusters. The clusters which are sampled up to external cluster regions really shows a flattening of the profiles (e.g., A2390, MS0451+02, MS1621+26), while the behavior of profiles for some others is still uncertain (e.g., MS1006+12).

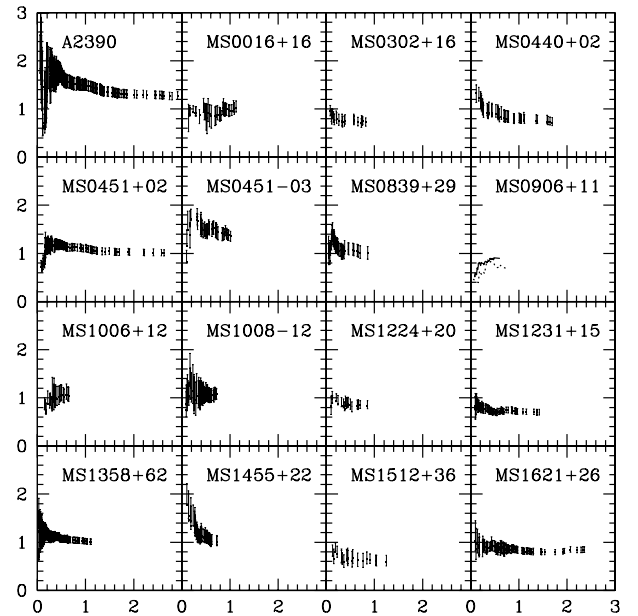


Fig. 3.— Integrated line-of-sight velocity dispersion profiles, where the dispersion at a given radius is  $\sigma_{rob}$  estimated by considering all galaxies within that radius. The bootstrap error bands at the 68% c.l. are shown. Distances on the  $x$ -axis are in units of  $h^{-1}\text{Mpc}$ , and the velocity dispersions on the  $y$ -axis are in units of  $10^3 \text{ km s}^{-1}$ . As for MS0906+11 the solid and dotted lines correspond to peak  $a$  and  $b$ , respectively (errorbars are omitted here for reasons of clarity).

In order to test the robustness of the  $\sigma_v$  computations, we also use three other estimators: (a) a weighted version of the robust estimate  $\sigma_{w-rob}$ , (b) the usual standard deviation  $\sigma_s$ , and (c) its weighted version  $\sigma_{w-s}$ . As for the weighted estimators, to each galaxy is associated a magnitude-dependent geometric weight, which has been introduced in order to account for the geometry of the field surveyed around each cluster and the magnitude completeness of the sample (cf. Yee, Ellingson, & Carlberg 1996 for further details). The result of the  $\sigma_v$  analysis are reported in Table 1 where we give for each cluster: the total number of galaxy redshifts,  $N_{tot}$ , available for each cluster (Column 2); the number of member galaxies found in peaks,  $N_m$ , as recognized by our interloper-removal algorithm (Column 3); the bi-weight mean cluster velocity (Column 4); the values of  $\sigma_{rob}$  with the relative bootstrap error (at 68% c.l.; Column 5); and the other three estimates of the velocity dispersion that we considered (Columns 6-8).

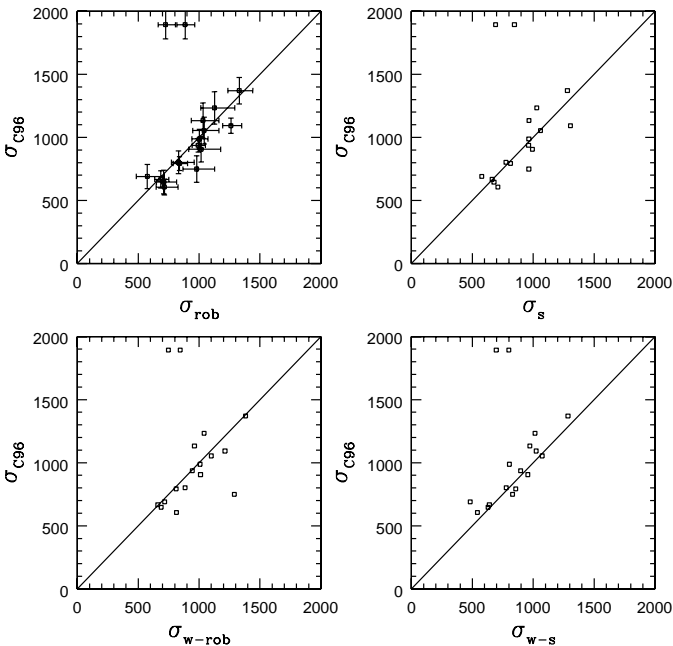


Fig. 4.— The comparison between line-of-sight velocity dispersions (in units of  $\text{km s}^{-1}$ ) as estimated by Carlberg et al. (1996),  $\sigma_{C96}$ , and the four types of estimates we obtain in this work (see text). The  $1\sigma$  bootstrap errorbars are shown only in the  $\sigma_{C96}-\sigma_{rob}$  comparison. The two very discrepant points refer to the two sub-clusters in which MS0906+11 has been divided.

In Figure 4 we compare our estimates of  $\sigma_v$  to those,  $\sigma_{C96}$ , provided by C96 and based on the explicit background subtraction algorithm. Apart from the exception of MS0906+11, which we divide into two subclumps, the present  $\sigma_v$  estimates show an overall agreement with  $\sigma_{C96}$ . We find that the median values of the ratio  $\sigma_v/\sigma_{C96}$  for the

different estimators lie in the range 0.96 – 1.04. In particular, it is  $\sigma_{rob}/\sigma_{C96} = 1.04^{+0.06}_{-0.07}$ , where errors are at 90% c.l. It is remarkable that different methods give  $\sigma_v$  which, on average, agree within  $\lesssim 10\%$ , thus confirming the result by Girardi et al. (1993) that different estimators of  $\sigma_v$  give statistically similar results on cluster samples. This supports the reliability of such cluster dynamical studies from optical observations.

Unless otherwise specified, we adopt in the following the  $\sigma_{rob}$  estimator, which is the most directly comparable to that used by F96 and G98.

We also show in Figure 5 the correlation between  $\sigma_v$  and bolometric  $X$ -ray luminosity for CNOC clusters (filled circles). This correlation is also compared to that obtained for local clusters by combining the XBACs sample (Ebeling et al. 1996) with the G98 sample of velocity dispersions (open circles).

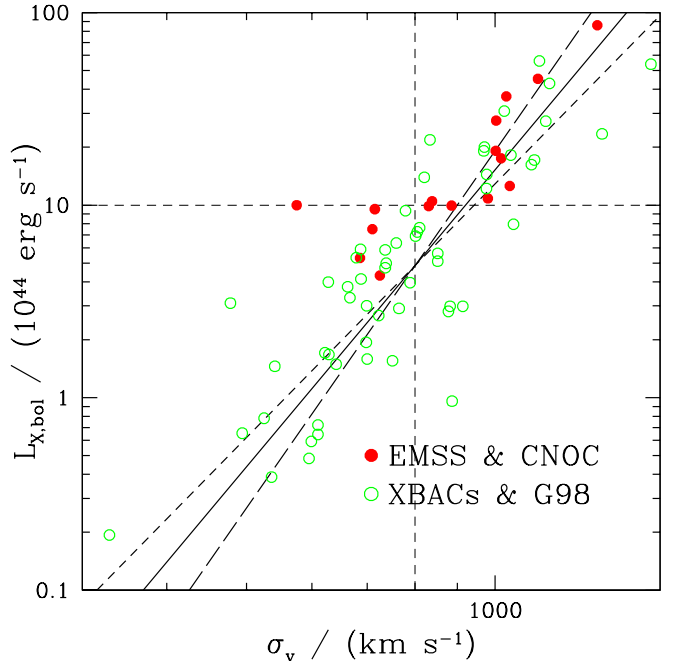


Fig. 5.— The  $L_{bol}-\sigma_v$  relation for local (open circles) and distant CNOC clusters (filled circles). For the local data, we show results for those clusters of the Girardi et al. (1998) sample, which are also included in XBACs (Ebeling et al. 1996). We restricted to those clusters whose  $\sigma_v$  is estimated at least with 30 galaxy redshifts. For CNOC clusters,  $X$ -ray luminosities have been taken from the EMSS (Henry et al. 1992). Short-dashed, long-dashed and continuous lines are the direct, inverse and bisector linear regression for the local data points. The light horizontal and vertical dashed lines indicate the  $L_{X,bol}$  and  $\sigma_v$  limits above which we select CNOC clusters for deriving cosmological constraints.

Bolometric luminosities for CNOC (XBACs) clusters,  $L_{X,bol}$ , have been estimated by multiplying luminosities in the [0.3–3.5] keV ([0.1–2.4] keV) energy band by a temperature-dependent bolometric correction factor. This

TABLE 1  
CLUSTER VELOCITY DISPERSIONS

Name	$N_{tot}$	$N_m$	$V$ km s <sup>-1</sup>	$\sigma_{rob}$ km s <sup>-1</sup>	$\sigma_{w-rob}$ km s <sup>-1</sup>	$\sigma_s$ km s <sup>-1</sup>	$\sigma_{w-s}$ km s <sup>-1</sup>
A2390	252	191	68608	1262 <sup>+89</sup> <sub>-68</sub>	1213	1306	1024
MS0016+16	65	41	164729	1127 <sup>+166</sup> <sub>-112</sub>	1042	1029	1014
MS0302+16	58	27	127333	710 <sup>+106</sup> <sub>-60</sub>	688	678	630
MS0440+02	78	47	58793	715 <sup>+113</sup> <sub>-68</sub>	815	709	542
MS0451+02	189	122	60057	1002 <sup>+72</sup> <sub>-61</sub>	1009	964	805
MS0451-03	74	46	161689	1330 <sup>+111</sup> <sub>-94</sub>	1382	1281	1286
MS0839+29	94	47	57818	980 <sup>+147</sup> <sub>-113</sub>	1289	964	831
MS0906+11a	92	50	52940	886 <sup>+78</sup> <sub>-68</sub>	845	846	799
MS0906+11b	92	40	49428	725 <sup>+82</sup> <sub>-61</sub>	749	691	697
MS1006+12	38	30	77965	1017 <sup>+161</sup> <sub>-103</sub>	1012	994	955
MS1008-12	84	69	91891	1042 <sup>+121</sup> <sub>-94</sub>	1101	1060	1074
MS1224+20	34	24	97508	831 <sup>+129</sup> <sub>-57</sub>	886	777	779
MS1231+15	120	77	70329	686 <sup>+65</sup> <sub>-50</sub>	660	663	640
MS1358+62	209	136	98404	1003 <sup>+61</sup> <sub>-52</sub>	1038	973	917
MS1455+22	68	51	76991	1032 <sup>+130</sup> <sub>-95</sub>	962	965	972
MS1512+36	84	26	11199	575 <sup>+138</sup> <sub>-90</sub>	717	577	483
MS1621+26	173	101	128182	839 <sup>+67</sup> <sub>-53</sub>	811	814	856

factor has been computed under the assumptions of pure bremsstrahlung ICM emission and power-law approximation for the Gaunt factor,  $g(E, kT) \propto (E/kT)^{-0.3}$ , which is quite accurate for  $kT > 2$  keV (cf. B99). Temperatures are available for all but two CNOC clusters, namely MS1231+15 and MS1621+26 (Lewis et al. 1999). For such two clusters they have been estimated from the velocity dispersion according to  $kT = (\sigma_v/350 \text{ km s}^{-1}) \text{ keV}$ . As for the double cluster MS0906+11, we assigned the same overall temperature,  $kT = 8$  keV, to both subclusters. The resulting bolometric correction factors range from 1.6 to 3.7. According to Fig. 5, it turns out that there is no appreciable evolution for the  $L_{X,bol}-\sigma_v$  relation, thus consistent with the lack of significant evolution in the  $L_{X,bol}-T$  relation at  $z \lesssim 0.4$  (e.g., Mushotzky & Scharf 1997) and also in agreement with the recent analysis by . The only outlier is MS1512+36, which is one of the two highly substructured objects that we discussed above. The solid line represents the bisector between the direct and the inverse log-log linear regression (short- and long-dashed lines, respectively) for local clusters. The resulting  $L_X-\sigma_v$  relation is given by

$$\log L_X = 5.1^{+1.2}_{-0.8} \log \sigma_v - 14.2^{+3.0}_{-2.2} \quad (1)$$

with a scatter  $\Delta_{L_X} = \Delta \log L_X / \log L_X \simeq 0.36$  around the best-fitting relation and in agreement with the recent analysis by Wu, Xue & Fang (1999). The upper and lower errors represent here the difference with respect to the direct and the inverse linear regression, respectively. Eq.(1) has been obtained by considering the 53 clusters of the

G98 sample, which have  $\sigma_v > 500 \text{ km s}^{-1}$  and at least 30 galaxy members (cf. G98). If  $T_X \propto \sigma_v^2$ , as expected under the assumption of isothermal gas and hydrostatic equilibrium, then eq.(1) would imply  $L_{X,bol} \propto T_X^{2.5}$  for the luminosity-temperature relation, a results which is not far from recent calibrations of the  $L_{X,bol}-T_X$  relation for rich clusters (e.g., Allen & Fabian 1998; Arnaud & Evrard 1999, and references therein).

## 4 CONSTRAINING $\Omega_m$

### 4.1 Modeling the $\sigma_v$ distribution

The starting point of this analysis is represented by the Press-Schechter (1974, PS hereafter) expression for the comoving number density, at redshift  $z$ , of virialized halos with mass in the range  $[M, M + dM]$ :

$$N(M, z) dM = \sqrt{\frac{2}{\pi}} \frac{\bar{\rho}}{M^2} \frac{\delta_c(z)}{\sigma_M} \left| \frac{d \log \sigma_M}{d \log M} \right| \times \exp\left(-\frac{\delta_c(z)^2}{2\sigma_M^2}\right) dM. \quad (2)$$

Here  $\bar{\rho}$  is the present-day average matter density and  $\delta_c(z)$  is the linear-theory overdensity extrapolated at the present time for a uniform spherical fluctuation collapsing at redshift  $z$ . It is convenient to express it as  $\delta_c(z) = \delta_{c,0}(z) [D(0)/D(z)]$ , where  $D(z)$  is the linear fluctuation growth factor (see, e.g., Peebles 1993). For a critical-density Universe,  $\delta_{c,0} = 1.686$  with a weak dependence on  $\Omega_m$ . We take for  $\Omega_m < 1$  the expression provided by

Lacey & Cole (1993) and Kitayama & Suto (1996). The quantity  $\sigma_M$  is the present day linear r.m.s. fluctuation within a sphere of radius  $R = (3M/4\pi\bar{\rho})^{1/3}$  and is specified by the power-spectrum,  $P(k)$ , of density fluctuations. We assume for  $P(k)$  the parametric CDM-like expression provided by Bardeen et al. (1986). Accordingly, its profile and amplitude are determined by the shape-parameter  $\Gamma$  ( $\simeq 0.2$  from the the observed galaxy distribution; e.g., Efstathiou, Bond & White 1992) and by  $\sigma_8$ , the r.m.s. fluctuation amplitude within a sphere of  $8 h^{-1}\text{Mpc}$  radius. The reliability of eq.(2) for predicting the mass distribution of virialized halos has been tested and debated at length in the literature (e.g., Lacey & Cole 1994; Bryan & Norman 1998; Gross et al. 1998; B99; Governato et al. 1999) and we refer to such papers for further details.

In order to convert the distribution of cluster masses into that of one-dimensional velocity dispersions,  $\sigma_v$ , we use the relation

$$M(\sigma_v) = \left( \frac{\sigma_v}{1129 f_\sigma \text{ km s}^{-1}} \right)^3 \left( \frac{\Delta_c(z)}{178} \right)^{-1/2} \times E^{-1}(z) \times 10^{15} h^{-1} M_\odot, \quad (3)$$

where  $E(z) = [(1+z)^3\Omega_m + (1+z)^2(1-\Omega_m-\Omega_\Lambda) + \Omega_\Lambda]^{1/2}$  and  $\Delta_c$  is the ratio between the average density within a virialized halo and the critical background density at  $z$  (e.g., Bryan & Norman 1998). It is  $\Delta_c = 178$  for  $\Omega_m = 1$  while the expression for  $\Omega_m < 1$  has been taken from Kitayama & Suto (1996). Eq.(3) corresponds to the case of an isothermal halo density profile for  $f_\sigma = 1$  (Binney & Tremaine 1987), with slightly smaller values,  $0.9 \lesssim f_\sigma \lesssim 1$ , for steeper profiles at the virial radius (e.g., Navarro, Frenk & White 1996). Since different halos have different dynamical histories, we expect that an intrinsic scatter,  $\Delta_M = \Delta M/M$ , should be present around eq.(3). Once the  $M$ - $\sigma_v$  relation and its scatter are calibrated, the distribution of velocity dispersions,  $N(\sigma_v)$ , is obtainable by convolving eq.(2) with a Gaussian distribution having dispersion  $\Delta_M$ .

In order to estimate  $f_\sigma$  and  $\Delta_M$ , we resort to  $N$ -body simulations, based on the Adaptive P3M code by Couchman (1991). We analyze two sets of simulations, which have been run for an Einstein-de-Sitter (EdS) model and for a flat low-density model with  $\Omega_m = 0.4$  ( $\Lambda 0.4$ ). Both models have been chosen to be consistent with the abundance of local clusters. Each simulation box is  $250 h^{-1}\text{Mpc}$  aside and five realizations have been run for each model. Such simulations have already been used by B99 to test the PS mass function and we refer to that paper for further details. Once clusters are identified,  $f_\sigma$  and  $\Delta_M$  are estimated from their  $M$ - $\sigma_v$  virial relation. The results of this analysis are reported in Figure 6, where we plot, at three different redshifts,  $f_\sigma$  and  $\Delta_M$  as a function of the cluster number density, lower  $n_{cl}$  corresponding to the population of richer clusters. We find that  $f_\sigma$  and  $\Delta_M$  are essentially independent of both the simulated models and the evolutionary stage. Only the EdS result on  $f_\sigma$  at  $z = 0.2$  for the smallest  $n_{cl}$  (i.e., for the most mas-

sive cluster population) shows a marginal departure from the general behavior. We checked that this is generated by one single cluster, appearing in one of the five realizations, which has an anomalous high  $\sigma_v$ . Based on this result, we adopt in the following the best fitting values,  $f_\sigma = 0.93$  and  $\Delta_M = 0.15$ .

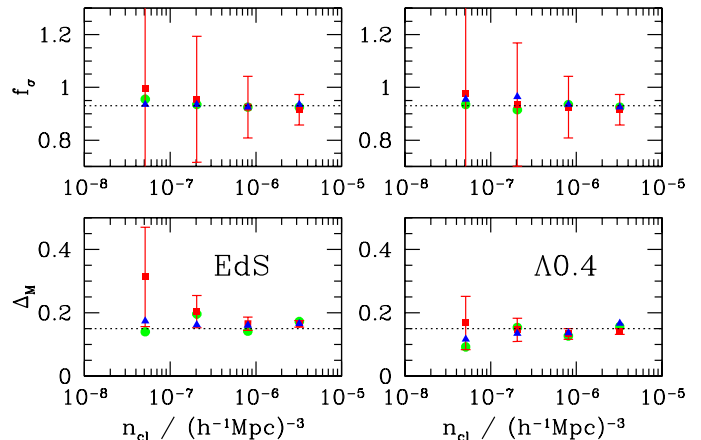


Fig. 6.— The normalization  $f_\sigma$  (upper panels) and the scatter  $\Delta_M$  (lower panels) for the  $M$ - $\sigma_v$  relation [cf. eq.(3)] from  $N$ -body simulations are plotted against the cluster number density. Left and right panels are for the EdS and the  $\Lambda 0.4$  model, respectively (see text). In each panel, circles, squares and triangles refer to the outputs at  $z = 0, 0.2, 0.6$ , respectively. Errorbars, which are reported only for the  $z = 0.2$  output, are  $1\sigma$  Poisson scatter.

#### 4.2 Maximum-likelihood analysis

In order to constrain cosmological parameters we compare the cluster distribution on the  $(\sigma_v, z)$  plane with model predictions for samples having the same completeness and selection criteria of the CNOC sample. A similar approach has been recently used by Eke et al. (1998) to follow the evolution of the cluster  $X$ -ray temperature function for the Henry (1997) sample, and by Borgani et al. (1998) to follow the evolution of the  $X$ -ray luminosity function in the ROSAT Deep Cluster Survey (Rosati et al. 1998).

This method is based on partitioning the  $(\sigma_v, z)$  plane into elements of size  $d\sigma_v dz$  and on computing the model probability  $\lambda(\sigma_v, z) d\sigma_v dz$  of observing a CNOC cluster with velocity dispersion  $\sigma_v$  at redshift  $z$ , given the completeness and selection criteria of the sample. If the bin width is small enough that such probabilities are always much smaller than unity, then the likelihood function  $\mathcal{L}$  of the observed cluster velocity dispersions and redshift is defined as the product of the probabilities of observing exactly one cluster in  $dz d\sigma_v$  at each of the  $(\sigma_{v,i}, z_i)$  positions occupied by the CNOC clusters, and of the probabilities of observing zero clusters in all the other differential ele-

ments of the  $(\sigma_v, z)$  plane. Assuming Poisson statistics for such probabilities, we obtain

$$\mathcal{L} = \prod_i \left[ \lambda(\sigma_{v,i}, z_i) dz d\sigma_v e^{-\lambda(\sigma_{v,i}, z_i) dz d\sigma_v} \right] \times \prod_{j \neq i} e^{-\lambda(\sigma_{v,j}, z_j) dz d\sigma_v}, \quad (4)$$

where the indices  $i$  and  $j$  run over the occupied and empty elements of the  $(\sigma_v, z)$  plane, respectively. Defining, as usual,  $S = -2\ln\mathcal{L}$ , and dropping all the terms which do not depend on the parameters of the cosmological model, we find

$$S = -2\ln\mathcal{L} = -2 \sum_i \ln[\lambda(\sigma_{v,i}, z_i)] + 2 \int dz \int d\sigma_v \lambda(\sigma_v, z), \quad (5)$$

where the integral is performed over the redshift and velocity dispersion intervals spanned by the cluster sample (see also Marshall et al. 1983).

The function  $\lambda(\sigma_v, z)$  is given by

$$\lambda(\sigma_v, z) = N(\sigma_v, z) \frac{dV(z)}{dz} f_{sky}, \quad (6)$$

where  $N(\sigma_v, z)$  is the comoving number density of clusters with velocity dispersion  $\sigma_v$  at redshift  $z$ ,  $dV(z)$  is the comoving volume element in the redshift interval  $[z, z + dz]$  and  $f_{sky}$  is the sky-coverage, i.e. the effective fraction of the sky surveyed by EMSS. In order to account for bootstrap errors in the  $\sigma_v$  estimates we compute  $N(\sigma_v, z)$  by convolving the Press–Schechter-based predictions with a 10% Gaussian-distributed relative scatter, which is representative of the statistical uncertainties in  $\sigma_v$  (cf. Table 1). Since  $f_{sky}$  for EMSS clusters depends on the detect-cell flux, we compute it for given  $\sigma_v$  and  $z$  by integrating over all the possible fluxes, thereby accounting for the scatter in the  $L_{bol}-\sigma_v$  correlation of eq.(1). In order to account for the fact that detect-cell fluxes are smaller than total cluster fluxes, we divide the latter by a factor 2.1, which has been shown by Henry et al. (1992) to be appropriate at least for clusters in the redshift range [0.22–0.33] (cf. their Figure 1).

A further selection effect that we have to account for in the estimate of the likelihood function is connected to the fact that, at a given  $\sigma_v$ , the  $X$ -ray luminosity- and flux-limit criteria cause faint clusters to be missed in the CNOC sample. In order to correct for this  $\sigma_v$ -incompleteness, we follow a similar procedure to that adopted by C97. We select those CNOC clusters which have  $\sigma_v > 800 \text{ km s}^{-1}$  and  $L_{X,bol} > 10^{45} \text{ erg s}^{-1}$ . Then we resort to a complete local cluster sample to estimate the fraction  $\mathcal{F}_{800}$  of all clusters with  $\sigma_v > 800 \text{ km s}^{-1}$ , which also satisfy the above luminosity selection. Finally, we correct for the  $\sigma_v$  incompleteness by multiplying by  $\mathcal{F}_{800}^{-1}$  the sum over the occupied cells in the r.h.s. of eq.(5).

To estimate  $\mathcal{F}_{800}$ , we cross-correlate the ENACS cluster sample (Katgert et al. 1998), which at  $z \lesssim 0.1$  is representative of the whole cluster population for  $\sigma_v > 800 \text{ km s}^{-1}$

(Mazure et al. 1996), with the XBACs (Ebeling et al. 1996), which includes all the Abell/ACO clusters identified in the ROSAT all-sky survey and is 80% complete for fluxes  $f_{[0.1-2.4]} > 5 \times 10^{-12} \text{ erg s}^{-1} \text{ cm}^{-2}$ . Since at  $z = 0.1$  this flux corresponds to a luminosity  $L_{X,[0.1-2.4]} \simeq 2 \times 10^{44} \text{ erg s}^{-1}$ , we are reasonably guaranteed that, for typical bolometric corrections, XBACs contains all the Abell-type clusters with  $L_{X,bol} > 10^{45} \text{ erg s}^{-1}$  in the redshift range covered by ENACS. Therefore,  $\mathcal{F}_{800}$  is given by the fraction of ENACS clusters with  $\sigma_v > 800 \text{ km s}^{-1}$  and belonging to the XBACs with  $L_{X,bol} > 10^{45} \text{ erg s}^{-1}$ . It turns out that ENACS contains 26 clusters with  $\sigma_v > 800 \text{ km s}^{-1}$ , out of which 6 have  $L_{X,bol} > 10^{45} \text{ erg s}^{-1}$ . Therefore, we obtain  $\mathcal{F}_{800}^{-1} = 4.3 \pm 2.0$ , where the uncertainty is the  $1\sigma$  Poissonian error. We note that using local data to estimate  $\mathcal{F}_{800}$  is consistent with the lack of significant evolution in the  $L_{X,bol}-\sigma_v$  relation shown in Fig. 5.

In their analysis, C97 used the data on  $L_X$  and  $\sigma_v$  by Edge & Stewart (1991) and found  $\mathcal{F}_{800}^{-1} = 2.0 \pm 1.0$ . The consequence of a smaller  $\mathcal{F}_{800}^{-1}$  is that a smaller fraction of clusters is expected to be lost below the luminosity limit. Therefore a smaller number of clusters with  $\sigma_v > 800 \text{ km s}^{-1}$  is expected at high redshift and a larger value of  $\Omega_m$  would be implied. This will be discussed on a more quantitative ground in §4.3 below.

Best estimates of the model parameters are obtained by minimizing  $S$  and confidence regions are estimated by allowing for standard increments  $\Delta S$ . Unless otherwise specified, in the following we will restrict our analysis only to the case of vanishing cosmological constant.

### 4.3 Results

Figure 7 shows constraints on the  $\sigma_8-\Omega_m$  plane taking  $\Gamma = 0.2$  for the power-spectrum shape (we checked that results are weakly dependent on  $\Gamma$  within the range allowed by galaxy clustering data; e.g., Peacock & Dodds 1994). Such results are based on adopting the unweighted robust estimator for  $\sigma_v$  (cf. Section 2) and taking only clusters with  $\sigma_v > 800 \text{ km s}^{-1}$  and  $L_{X,bol} > 10^{45} \text{ erg s}^{-1}$ . The plotted iso-likelihood contours corresponds to  $1\sigma$ ,  $2\sigma$  and  $3\sigma$  confidence levels. The dashed curves are the  $\sigma_8-\Omega_m$  relation coming from the local cluster abundance and correspond to  $\tilde{\sigma}_8 = 0.50, 0.55$  and  $0.60$ , while the shape of the  $\sigma_8-\Omega_m$  relation is that provided by Girardi et al. (1998a).

Both the small number of clusters on which the analysis is based and the limited leverage in redshift allow a rather high level of degeneracy in the  $\sigma_8-\Omega_m$  plane. As expected, more stringent constraints on  $\Omega_m$  come by combining the results from CNOC clusters with those from the local cluster abundance. Taking  $\tilde{\sigma}_8 = 0.55$ , we find  $\Omega_m = 0.65_{-0.08}^{+0.13}$  (at the  $2\sigma$  c.l. for one significant parameter), thus ruling out a critical density model at a high confidence level (if  $\Omega_\Lambda = 1 - \Omega_m$ , then this result changes into  $\Omega_m = 0.53_{-0.12}^{+0.16}$ ). However, the variation of the best-fitting  $\Omega_m$  as  $\tilde{\sigma}_8$  is increased from 0.5 to 0.6 is much larger



than internal statistical uncertainties; indeed, we find that  $\Omega_m = 0.35^{+0.10}_{-0.07}$  and  $1.05^{+0.20}_{-0.14}$  for  $\tilde{\sigma}_8 = 0.5$  and  $0.6$ , respectively. Therefore, although uncertainties from the local cluster abundance are believed to be rather small, they propagate into large uncertainties in the determination of  $\Omega_m$  from distant cluster data (cf. also Colafrancesco, Mazzotta & Vittorio 1997). This is due to the fact that CNOC clusters are rather rich systems and, therefore, probe the high-mass tail of the mass function, which is very sensitive to the power spectrum normalization. On the one hand, this confirms the good news that results from a small number of clusters with precise determinations of  $\sigma_v$  can be used to constrain  $\Omega_m$ , once they are combined with local data. On the other hand, the bad news is that current uncertainties in the local cluster abundance are still large enough to prevent placing strong constraints on the density parameter. We regard this as a general problem one has to face with, even assuming that the analysis of high- $z$  sample is perfectly under control.

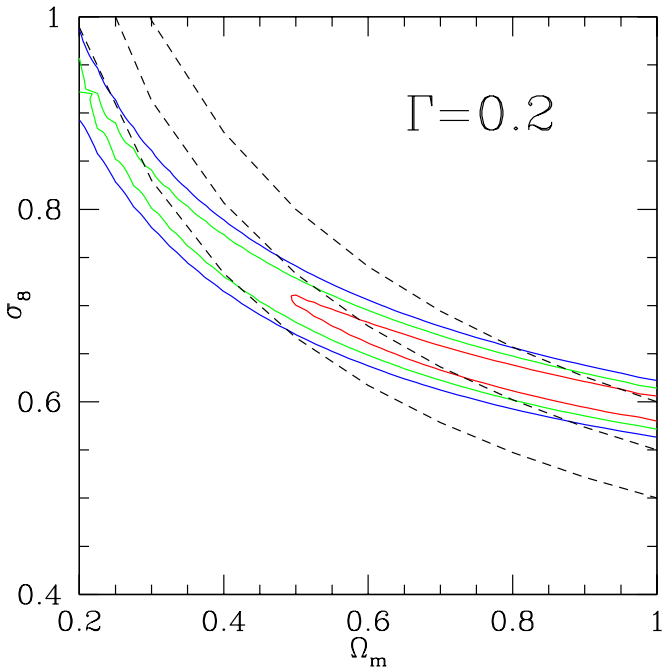


Fig. 7.— Iso-likelihood contours on the  $(\sigma_8, \Omega_m)$  plane for  $\Gamma = 0.2$ . Results refer to the reference analysis method, as described in Section 4.3. Iso-likelihood contours are for  $\Delta S = 2.30, 6.17$  and  $11.8$ , which corresponds to  $1\sigma$ ,  $2\sigma$  and  $3\sigma$  c.l. for two significant fitting parameters. The three dashed curves are the  $\sigma_8$ - $\Omega_m$  relation from the local cluster abundance, for  $\tilde{\sigma}_8 = 0.50, 0.55$  and  $0.60$ , from lower to upper curves, while the scaling is taken from Girardi et al. (1998b).

A further source of uncertainty in constraining  $\Omega_m$  arises from the correction for the  $\sigma_v$ -incompleteness. We find that, as  $\mathcal{F}_{800}$  varies, within its  $1\sigma$  range, from 2.3 to 6.3 (cf. §4.2), the best-fitting  $\Omega_m$  decreases from  $\simeq 0.9$  to  $\simeq 0.5$ . Therefore, the effect of this uncertainty is also non-

negligible and calls for the need of a substantially larger number of clusters with both  $L_X$  and  $\sigma_v$  determinations to suppress the Poissonian uncertainty in the estimate of  $\mathcal{F}_{800}$ .

Furthermore, we note from Fig. 5 that there are two clusters, MS1224+20 and MS0906+11a, whose values of  $L_{X,bol}$  are only slightly below the adopted luminosity limit. Owing to residual uncertainties in the bolometric correction, one may wonder by how much results would change if such clusters were included in the analysis. In this case, we find that, for  $\tilde{\sigma}_8 = 0.55$ , the best-fitting  $\Omega_m$  only decreases by 0.06.

In order to clarify the crucial role of the low- $z$  normalization for tracing the redshift evolution of the cluster abundance, we compare in Figure 8 the comoving cluster number density, with  $\sigma_v > 800 \text{ km s}^{-1}$ , to model predictions for a critical and an open low-density model, assuming different normalizations from the local cluster abundance. The estimate of the CNOC cluster abundance is obtained by dividing the nine selected clusters into two redshift intervals,  $0.15 \leq z \leq 0.30$  and  $0.30 \leq z \leq 0.55$ , which contain five and four clusters, respectively. Number densities are then estimated by applying the  $1/V_{max}$  method (Avni & Bahcall 1978) and following the same procedure as C97. Apart from the details of the model constraints, which are in general agreement with the results from Fig. 7, this plot gives a visual impression of why a change in the normalization from the local cluster abundance turns into a change of the preferred  $\Omega_m$  value. For instance,  $n(> 800, z = 0) \simeq 3 \times 10^{-6} (h^{-1} \text{Mpc})^{-3}$ , as coming from the virial analysis of local clusters (e.g., Mazure et al. 1996; Fadda et al. 1996), would be consistent with a critical density Universe, while  $n(> 800, z = 0) \simeq 10^{-6} (h^{-1} \text{Mpc})^{-3}$ , as implied by the estimates of the local X-ray temperature function by Eke et al. (1996) and Markevitch (1998), would instead favor a low-density Universe.

Since this is not the first analysis aimed at constraining  $\Omega_m$  and  $\sigma_8$  from the CNOC cluster abundance evolution (C97; Bahcall et al. 1997), it is worth comparing our results to those from such previous analyses. C97 provided the number density of clusters with mass within a physical radius of  $1.5 h^{-1} \text{Mpc}$  above a given limit by dividing the CNOC sample into two redshift bins. It is interesting to note that, despite the value of  $\mathcal{F}_{800}$  used in that analysis is about twice as large than ours, their results prefer lower  $\Omega_m$  (cf. Bahcall et al. 1998, for a stronger claim for a low density parameter,  $\Omega_m \simeq 0.3$ , from CNOC clusters). The reason for this difference is mainly due to the fact that C97 use a fixed normalization for the local cluster abundance. In particular, they noticed that, if ENACS velocity dispersions are thought to be overestimated by 13%, then the implied cluster abundance is compatible with that found by Eke et al. (1996) from the X-ray temperature function. In fact, the number density of local clusters with  $\sigma_v > 800 \text{ km s}^{-1}$ , as given by C97, would be compatible with  $\tilde{\sigma}_8 = 0.5$ . In view of the good agreement we found here between velocity disper-

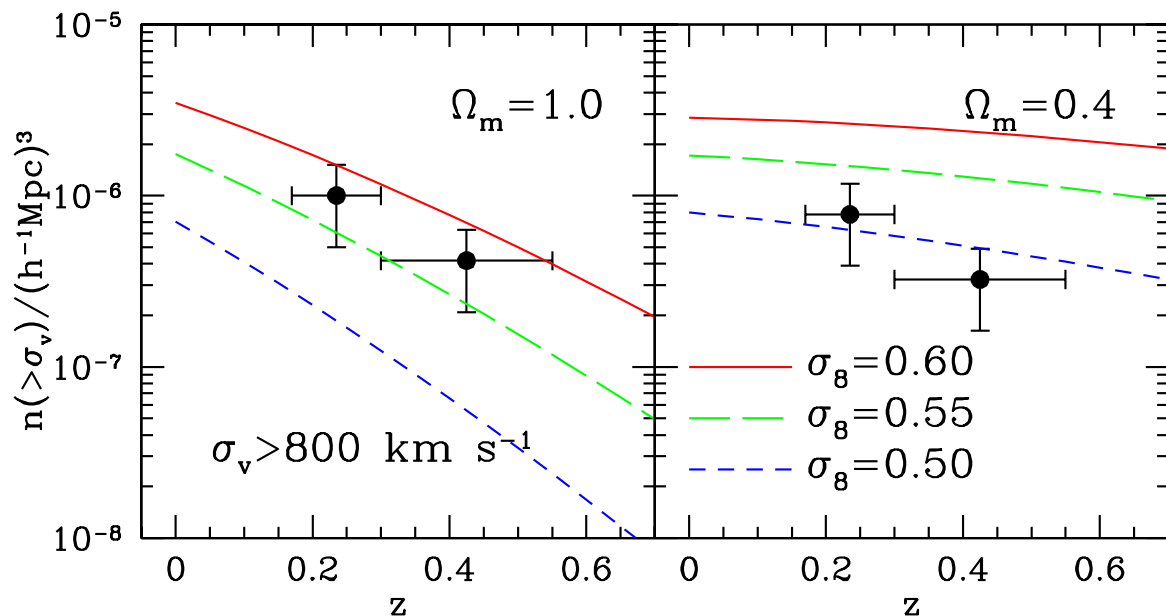


Fig. 8.— The redshift evolution of the comoving number density of CNOC clusters with  $\sigma_v > 800 \text{ km s}^{-1}$ , compared with model predictions. Left and right panels refer to a critical-density and to an open model with  $\Omega_m = 0.4$ , respectively. In each panel, the three different curves refer to three different normalizations from the local cluster abundance. We assume  $\Gamma = 0.2$  for the shape parameter of the power spectrum. The filled dots are the CNOC cluster number density in two redshift bins (see text). Vertical errorbars are  $1\sigma$  Poissonian uncertainties in  $n(>\sigma_v)$ , while horizontal errorbars indicate the extent of the redshift bins.

sions estimated with the explicit background subtraction and with the method applied to ENACS clusters, we argue that there is no evidence that ENACS velocity dispersions should be overestimated.

## 5 CONCLUSIONS

We analyzed the internal velocity dispersions,  $\sigma_v$ , of CNOC clusters (e.g., Yee, Ellingson & Carlberg 1996), by applying the algorithm originally developed by Fadda et al. (1996, F96; cf. also Girardi et al. 1998b, G98) for the analysis of local clusters. After removing interlopers, we applied four different  $\sigma_v$  estimators. By using the robust estimator, we found that for  $\sigma_v > 800 \text{ km s}^{-1}$  and  $L_{X,bol} > 10^{45} \text{ erg s}^{-1}$  the CNOC sample contains nine clusters, on which we base our analysis. In order to account for the clusters that we miss with respect to an ideal sample complete for  $\sigma_v > 800 \text{ km s}^{-1}$ , we resort to local data in order to reliably estimate the fraction  $\mathcal{F}_{800}$  of clusters that in such a sample have  $L_{X,bol} > 10^{45} \text{ erg s}^{-1}$ . The resulting  $\sigma_v$  are used to trace the evolution of the cluster abundance in the  $0.17 \lesssim z \lesssim 0.55$  redshift range probed by the CNOC sample, with the purpose of placing constraints on the  $\sigma_8$ - $\Omega_m$  plane. Such constraints can then be combined with results from the local cluster abundance to constrain the cosmological density parameter.

The main results of our analysis can be summarized as follows.

- (a) The explicit background subtraction method applied by Carlberg et al. (1996, C96) on CNOC clusters

provides  $\sigma_v$  estimates which are fully consistent with those provided by the method applied in this paper. For instance, we find that the median of the ratio between the robust estimator and the C96 results is  $\sigma_{rob}/\sigma_{C96} = 1.04^{+0.06}_{-0.07}$ .

- (b) Current uncertainties in the  $\sigma_8$ - $\Omega_m$  relation from the local cluster abundance are still large enough not to allow CNOC data to distinguish to a high confidence level among a low-density Universe with  $\Omega_m \simeq 0.3$  and a critical density scenario.

Far from meaning that the evolution of the cluster abundance can hardly be used to place significant constraints on cosmological parameters, the results of our analysis anyway indicate that the situation is more complex than sometimes suggested. Somewhat surprisingly, the availability of precise cluster mass measurements at high redshift through both  $\sigma_v$  and  $X$ -ray temperature measurements may be only of partial help in increasing the strength of the constraints unless (a) systematic uncertainties in the local mass-function are reduced at a  $\lesssim 10\%$  level, and (b) the completeness criteria of high- $z$  cluster samples are well under control.

We acknowledge stimulating discussions with Neta Bahcall, Andrea Biviano, Alain Blanchard, Isabella Gioia, Michael Gross, Simon Morris and Joel Primack. We thank Hugh Couchman for the sharing of his Adaptive P3M N-body code. SB and MG acknowledge SISSA in Trieste for its hospitality during the preparation of this work.

## REFERENCES

- Adami, C., Mazure, A., Biviano, A., Katgert, P., & Rhee, G. 1998, *A&A*, 331, 493
- Allen, S.W., & Fabian, A.C. 1998, *MNRAS*, 297, 63
- Arnaud, K.A., & Evrard, A.E. 1999, *MNRAS*, 305, 631
- Avni, Y., & Bahcall, J.N. 1980, *ApJ*, 235, 694
- Bahcall, N.A., Fan, X., & Cen, R. 1997, *ApJ*, 485, 53
- Bardeen, J.M., Bond J.R., Kaiser N., & Szalay, A.S. 1986, *ApJ*, 304, 15
- Beers, T.C., Flynn, K., & Gebhardt, K. 1990, *AJ*, 100, 32
- Binney, J., & Tremaine, S. 1987, *Galactic Dynamics* (Princeton: Princeton University Press)
- Borgani, S., Gardini, A., Girardi, M., & Gottlöber, S. 1997, *NewA*, 2, 119
- Borgani, S., Rosati, P., Tozzi, P., & Norman, C. 1998, in Proceedings of the Sesto Conference on "Observational Cosmology: the Development of Galaxy Systems", eds. G. Giuricin, M. Mezzetti and P. Salucci, p.51
- Borgani, S., Rosati, P., Tozzi, P., & Norman, C. 1999, *ApJ*, 517, 40
- Bryan, G.L., & Norman M.L. 1998, *ApJ*, 495, 80
- Carlberg, R.G., Yee, H.K.C., Ellingson, E., Abraham, R., Gravel, P., Morris, S., & Pritchet, C.J. 1996, *ApJ*, 462, 32 (C96)
- Carlberg, R.G., Yee, H.K.C., & Ellingson, E. 1997a, *ApJ*, 478, 462
- Carlberg, R.G., Morris, S.L., Yee, H.K.C., & Ellingson, E. 1997b, *ApJ*, 479, L19 (C97)
- Colafrancesco, S., Mazzotta, P., & Vittorio, N. 1997, *ApJ*, 488, 566
- Couchman, H.M.P. 1991, *ApJ*, 368, L23
- Danese, L., De Zotti, C., & di Tullio, G. 1980, *A&A*, 82, 322
- den Hartog R., & Katgert, P. 1996, *MNRAS*, 279, 349
- Donahue, M., Voit, G.M., Gioia, I., Luppino, G., Hughes, J.P., & Stocke, J.T. 1998, 502, 550
- Ebeling, H., Voges, W., Böhringer, H., Edge, A.C., Huchra, J.P., & Briel, U.G. 1996, *MNRAS*, 281, 799
- Edge, A.C., & Stewart, G.C. 1991, *MNRAS*, 252, 428
- Efstathiou, G., Bond, J.R., & White, S.D.M. 1992, *MNRAS*, 258, 1p
- Eke, V.R., Cole, S., & Frenk, C.S. 1996, *MNRAS*, 282, 263
- Eke, V.R., Cole, S., Frenk, C.S., & Henry, J.P. 1998, *MNRAS*, 298, 114
- Fadda, D., Girardi, M., Giuricin, G., Mardirossian, F., & Mezzetti, M. 1996, *ApJ*, 473, 670
- Gioia, I.M., Henry, H.P., Maccacaro, T., Morris, S.L., Stocke, J.T., & Walter, A. 1990, *ApJ*, 356, L35
- Girardi, M., Biviano, A., Giuricin, G., Mardirossian, F., & Mezzetti, M. 1993, *ApJ*, 404, 38
- Girardi, M., Borgani, S., Giuricin, G., Mardirossian, F., & Mezzetti, M., 1998a, *ApJ*, 506, 45
- Girardi, M., Giuricin, G., Mardirossian, F., Mezzetti, M., & Boschini, W. 1998b, *ApJ*, 505, 74 (G98)
- Governato, F., Babul, A., Quinn, T., Tozzi, P., Baugh, C.M., Katz, N., & Lake, G. 1998, *MNRAS*, in press, astro-ph/9810198
- Gross, M.A.K., Somerville, R. S., Primack, J.R., Holtzman, J., & Klypin A. 1998, *MNRAS*, 301, 81
- Henry, J.P., 1997, *ApJ*, 489, L1
- Henry, J.P., Gioia, I.M., Maccacaro, T., Morris, S.L., Stocke, J.T., & Wolter A. 1992, *ApJ*, 386, 408
- Katgert, P., Mazure, A., den Hartog, R., Adami, C., Biviano, A., & Perea, J. 1998, *A&AS*, 129, 399
- Kitayama, T., & Suto, Y., 1996, *ApJ*, 469, 480
- Kitayama, T., & Suto, Y., 1997, *ApJ*, 490, 557
- Lacey, C.G., & Cole, S. 1993, *MNRAS*, 262, 627
- Lacey, C.G., & Cole, S. 1994, *MNRAS*, 271, 676
- Lewis A.D., Ellingson E., Morris S.L., & Carlberg, R.G., 1999, *ApJ*, 517, 587
- Luppino, G.A., & Gioia, I. 1995, *ApJ*, 445, L77
- Marshall, H.L., Avni, Y., Tananbaum, H., & Zamorani, G. 1983, *ApJ*, 269, 35
- Markevitch, M. 1998, *ApJ*, 504, 27
- Mazure, A., et al. 1996, *A&A*, 310, 31
- Merritt, D. 1987, *ApJ*, 313, 121
- Mushotzky, R.F., & Scharf, C.A. 1997, *ApJ*, 482, L13
- Navarro, J.F., Frenk, C.S., & White, S.D.M. 1996, *ApJ*, 462, 563
- Oukbir, J., & Blanchard, A. 1992, *A&A*, 252, L21
- Oukbir, J., Bartlett, J.G., & Blanchard, A. 1997, *A&A*, 320, 365
- Peacock, J.A., & Dodds, S.J. 1994, *MNRAS*, 267, 1020
- Peebles, P.J.E. 1980, *The Large-Scale Structure of the Universe* (Princeton: Princeton University Press)
- Peebles, P.J.E. 1993, *Physical Cosmology* (Princeton: Princeton University Press)
- Pen, U.L. 1998, *ApJ*, 498, 60
- Pisani, A. 1993, *MNRAS*, 265, 706
- Press, W.H., & Schechter, P. 1974, *ApJ*, 187, 425 (PS)
- Reichart, D.E., Nichol, R.C., Castander, F.J., Burke, D.J., Romer, A.K., Holden, B.P., Collins, C.A., & Ulmer, M.P. 1998, *ApJ*, 518, 521
- Rosati, P., Della Ceca, R., Burg, R., Norman, C., & Giacconi, R., 1995, *ApJ*, 445, L11
- Rosati, P., Della Ceca, R., Burg, R., Norman, C., & Giacconi, R., 1998, *ApJ*, 492, L21
- Rosati, P., Stanford, S.A., Eisenhardt, P.R., Elston, R., Spinrad, H., Stern, D., Dey, A. 1999, *AJ*, in press, preprint astro-ph/9903381
- Sadat, R., Blanchard, A., & Oukbir, J. 1998, *A&A*, 329, 21
- Viana, P.T.P., & Liddle, A.R. 1999, *MNRAS*, 303, 535
- White, S.D.M., Efstathiou, G., & Frenk, C.S. 1993, *MNRAS*, 262, 1023
- Wu, X.P., Xue, Y.J., & Fang, L.Z. 1999, *ApJ*, in press, preprint astro-ph/9905106
- Yahil A., & Vidal, N.V. 1977, *ApJ*, 214, 347
- Yee, H.K.C., Ellingson, E., & Carlberg, R.G. 1996, *ApJS*, 102, 269
- Zabludoff, A.I., Huchra, J.P., & Geller, M.J. 1990, *ApJS*, 74, 1